Spectrally precoded OTFS: Delay-Doppler detection

Vahid Vahidpour, Roberto López-Valcarce
atlanTTic Research Center, Universidade de Vigo, Vigo, Spain
Email: {vahidpour,valcarce}@gts.uvigo.es

***Abstract*—Similarly to other multicarrier-based schemes, orthogonal time-frequency space (OTFS) modulation suffers from high out-of-band radiation (OBR) causing adjacent channel interference. Although it is possible to apply well-known techniques such as spectral precoding in the time-frequency domain, which is effective toward OBR reduction, for OTFS the impact in terms of bit error rate (BER) degradation at the receiver can be significant. We enhance maximum ratio combining detection for spectrally precoded OTFS by introducing an iterative delay-Doppler domain scheme specifically designed for this setting. Simulation results show that the proposed approach significantly reduces OBR and improves BER performance compared to state-of-the-art detectors across various precoding methods, modulation orders, and frame sizes.**

***Index Terms*—OTFS, delay-Doppler, high mobility, out-of-band radiation, spectral precoding.**

I. Introduction

Reliable communication in high-mobility environments will be crucial in future-generation networks. While Orthogonal Frequency Division Multiplexing (OFDM) struggles with Doppler effects, Orthogonal Time-Frequency-Space (OTFS) modulation, operating in the delay-Doppler (DD) domain, offers superior robustness in time-varying channels [1]. Ideally pulsed OTFS systems were introduced in [2] to mitigate inter-carrier and inter-symbol interference (ICI/ISI) in the time-frequency (TF) domain, enhancing receiver performance. However, these systems are impractical. As an alternative, [3] shows that OTFS with rectangular pulse shaping and ICI/ISI cancellation achieves similar error performance but suffers from significant out-of-band radiation (OBR), leading to adjacent channel interference (ACI).

Over the years, a number of techniques have been proposed for mitigating spectral leakage in rectangularly pulsed OFDM, including filtering [4], time-domain windowing [5], [6], active interference cancellation (AIC) [7], [8], and spectral precoding [9]–[12]. While effective for OFDM, their application to OTFS is challenging due to waveform alterations affecting demodulation. Time-domain windowing for cyclic prefix-based OTFS (CP-OTFS, [13]) was proposed in [14], but the required receiver modifications in high-mobility channels were not specified. In [15], spectral precoding is introduced to mitigate sidelobes and reduce PAPR, with enhancements presented in [16]. The detection process employs time-domain precoder-aware linear minimum mean square error (LMMSE) equalization, followed by spectral decoding and symbol decisions in the DD domain; however, the resulting bit error rate (BER) degradation was significant.

Since maximum ratio combining (MRC) detection has been shown to achieve near-optimal performance in OTFS with reasonable complexity [17], [18], the authors explored in [19] the suitability of delay-time (DT) MRC detection for spectrally precoded OTFS. It was found that, while spectral shaping does reduce OBR, and the BER performance was indeed better than that of time-domain LMMSE equalization, a BER penalty still remained. Here we study the possibility of applying the iterative MRC detector in the DD domain under spectral precoding, and present the corresponding required modifications. The main contributions are summarized as follows:

- We examine spectral precoding, including orthogonal and AIC precoders, in the TF domain to mitigate high OBR in CP-OTFS.
- We propose a novel iterative DD-domain MRC detection scheme integrating spectral precoding.
- We show that the proposed method reduces OBR while outperforming state-of-the-art detectors across precoding schemes, modulation orders, and frame sizes.

Notation: a, $\mathbf{a}$, and $\mathbf{A}$ represent scalar, vector and matrix, resp.; $\mathbf{A}^{\mathsf{T}}$, $\mathbf{A}^{\mathsf{H}}$, $\mathbf{A}^{\dagger}$ denote transpose, conjugate transpose, and pseudoinverse of $\mathbf{A}$, resp.; $\mathbb{A}$ and $\mathbb{C}$ denote the constellation set and the complex number field. The m-th column of the identity matrix $\mathbf{I}$ is denoted as $\mathbf{e}_m$; $\mathsf{tr}(\mathbf{A})$ is the trace of $\mathbf{A}$, while $\mathsf{vec}(\mathbf{A})$ and $\mathsf{unvec}(\mathbf{a})$ denote column-wise vectorization and reshaping. $\mathbf{F}_M$ is the unitary M-point Discrete Fourier transform (DFT) matrix. $[a]_M$ denotes a modulo M. $\mathsf{DEC}\{\cdot\}$ is the entry-wise hard-decision operator for constellation $\mathbb{A}$.

II. System Model

A. CP-OTFS Transmitter

Consider the spectrally-precoded CP-OTFS transmitter shown in Fig. 1. Let $\mathbf{Q} \in \mathbb{A}^{D\times N}$ denote the data matrix of QAM symbols to transmit in a frame, set in the DD domain. A DD-domain spectral precoding matrix $\mathbf{G}_{\mathrm{DD}} \in \mathbb{C}^{M\times D}$ with $M \geq D$ is applied to the QAM data, yielding the DD-domain precoded frame $\mathbf{X}_{\mathrm{DD}} \in \mathbb{C}^{M\times N}$ as

$$\mathbf{X}_{\mathrm{DD}} = \mathbf{G}_{\mathrm{DD}}\mathbf{Q}. \tag{1}$$

The variables M and N represent the number of bins along the delay and the Doppler axes, respectively. The precoding redundancy and rate are $R = M - D$ and $\rho = D/M \leq 1$, resp. The inverse symplectic finite Fourier transform (ISFFT) [2] is then applied to obtain the TF-domain data matrix $\mathbf{X}_{\mathrm{TF}}$:

$$\mathbf{X}_{\mathrm{TF}} = \mathbf{F}_M\mathbf{X}_{\mathrm{DD}}\mathbf{F}_N^{\mathsf{H}}. \tag{2}$$

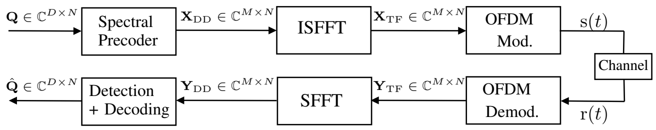

Fig. 1: OTFS system block diagram.

The operation of the OFDM modulator can be modeled as follows. First, an M-point IDFT is applied to yield the DT-domain matrix $\mathbf{X}_{\rm DT} \in \mathbb{C}^{M\times N}$:

$$\mathbf{X}_{\rm DT} = \mathbf{F}_M^{\mathsf{H}} \mathbf{X}_{\rm TF} = \mathbf{X}_{\rm DD} \mathbf{F}_N^{\mathsf{H}}, \tag{3}$$

and then a CP of length l_g is prepended to $\mathbf{X}_{\rm DT}$ to generate $\mathbf{X}_{\rm DT,CP} \in \mathbb{C}^{(M+l_g)\times N}$

$$\mathbf{X}_{\rm DT,CP} = \mathbf{A}_{\rm CP}\mathbf{X}_{\rm DT}, \quad \text{with } \mathbf{A}_{\rm CP} = \begin{bmatrix} \mathbf{0} & \mathbf{I}_{l_g} \\ \mathbf{I}_M & \end{bmatrix}, \tag{4}$$

where $\mathbf{A}_{\rm CP} \in \mathbb{C}^{(M+l_g)\times M}$ is the CP insertion matrix. Finally, the columns of $\mathbf{X}_{\rm DT,CP}$ are concatenated to construct the transmit vector $\mathbf{s} \in \mathbb{C}^{(M+l_g)N}$ as follows:

$$\mathbf{s} = \mathsf{vec}(\mathbf{X}_{\rm DT,CP}) \,. \tag{5}$$

The continuous-time OTFS signal $\mathrm{s}(t)$ is then to be synthesized from the samples in $\mathbf{s}$, with associated rate $\frac{1}{T}$ samples/s. In practice, the sample rate is first increased by a factor $F > 1$ to $\frac{F}{T}$ samples/s and then fed to the digital-to-analog converter (DAC). This relaxes the requirements of the DAC interpolation filters. Consequently, the subcarrier spacing is $\Delta_f = \frac{1}{MT}$ Hz, and the useful symbol duration (i.e., excluding the CP duration $T_g = l_g T$) is $T_u = MT$. Alternatively, an K-point IFFT with $K = FM$ can be used while preserving the subcarrier spacing, *i.e.,* $\frac{F}{KT} = \frac{1}{MT}$ [20].

B. Receiver

At the receiver end, the continuous-time channel output $\mathrm{r}(t)$ is sampled at $\frac{1}{T}$ samples/s, and then the CP is removed to yield the received discrete-time vector $\mathbf{r} \in \mathbb{C}^{NM}$. The corresponding DT-domain received matrix $\mathbf{Y}_{\rm DT} \in \mathbb{C}^{M\times N}$ is obtained as

$$\mathbf{Y}_{\rm DT} = \mathsf{unvec}(\mathbf{r}) \,. \tag{6}$$

The TF-domain matrix $\mathbf{Y}_{\rm TF} \in \mathbb{C}^{M\times N}$ is obtained from $\mathbf{Y}_{\rm DT}$ via M-point DFT:

$$\mathbf{Y}_{\rm TF} = \mathbf{F}_M \mathbf{Y}_{\rm DT}. \tag{7}$$

The symplectic finite Fourier transform (SFFT) is then applied to yield the DD-domain matrix $\mathbf{Y}_{\rm DD} \in \mathbb{C}^{M\times N}$

$$\mathbf{Y}_{\rm DD} = \mathbf{F}_M^{\mathsf{H}} \mathbf{Y}_{\rm TF} \mathbf{F}_N = \mathbf{Y}_{\rm DT} \mathbf{F}_N. \tag{8}$$

C. Delay-Doppler Domain Channel

The multipath channel response can typically be represented in the delay-Doppler domain as [2]:

$$\mathrm{h_c}(\tau,\nu) = \sum_{\gamma=1}^{L} \mathrm{g}_\gamma \delta(\tau - \tau_\gamma)\delta(\nu - \nu_\gamma) \tag{9}$$

where $\delta(\cdot)$ is the Dirac delta function, L is the number of propagation paths, and g_γ, τ_γ and ν_γ are the complex gain, delay, and Doppler shift for the γ-th path, resp. One has

$$\tau_\gamma = \frac{\ell_\gamma}{M\Delta_f} \le \tau_{\max}, \quad \nu_\gamma = \frac{\kappa_\gamma}{NT_{\rm u}}, \; |\nu_\gamma| \le \nu_{\max} \tag{10}$$

where $\ell_\gamma, \kappa_\gamma \in \mathbb{R}$ are the normalized delay and normalized Doppler shift, respectively. The maximum normalized delay is given by $\ell_{\max} = M\Delta_f \tau_{\max}$. We assume $\ell_{\max} < l_g \ll M$ and $\nu_{\max} < \Delta_f/2$, so that the channel is underspread, *i.e.,* $\tau_{\max}\nu_{\max} \ll 1$. The channel Doppler response is $\nu_\ell(\kappa) = g_\gamma$ if $(\ell,\kappa) = (\ell_\gamma,\kappa_\gamma)$, and zero otherwise. For convenience, we define the set of normalized delays $\mathcal{L} = \{\ell_1,\ldots,\ell_L\}$, as well as the index sets $\mathcal{M} = \{0,1,\ldots,M-1\}$, $\mathcal{N} = \{0,1,\ldots,N-1\}$.

D. Input-Output Relation in Delay-Doppler Domain

For $m \in \mathcal{M}$, let $\mathbf{x}_m, \mathbf{y}_m \in \mathbb{C}^N$, respectively, denote the transmitted and received symbol vectors along the Doppler axis. These are the columns of $\mathbf{X}_{\rm DD}^{\mathsf{T}}$ and $\mathbf{Y}_{\rm DD}^{\mathsf{T}}$, so that

$$\mathbf{x} = \mathsf{vec}\Big(\mathbf{X}_{\rm DD}^{\mathsf{T}}\Big) = [\mathbf{x}_0^{\mathsf{T}},\cdots,\mathbf{x}_{M-1}^{\mathsf{T}}]^{\mathsf{T}} \in \mathbb{C}^{NM}, \tag{11}$$

$$\mathbf{y} = \mathsf{vec}\Big(\mathbf{Y}_{\rm DD}^{\mathsf{T}}\Big) = [\mathbf{y}_0^{\mathsf{T}},\cdots,\mathbf{y}_{M-1}^{\mathsf{T}}]^{\mathsf{T}} \in \mathbb{C}^{NM}. \tag{12}$$

Additionally, define $\mathbf{w} = [\mathbf{w}_0^{\mathsf{T}},\cdots,\mathbf{w}_{M-1}^{\mathsf{T}}]^{\mathsf{T}}$ as the independent and identically distributed (i.i.d.) AWGN with variance σ_w^2. The CP-OTFS DD domain input-output model is [21]

$$\mathbf{y} = \mathbf{H}\mathbf{x} + \mathbf{w}. \tag{13}$$

For $m \in \mathcal{M}$ and $l \in \mathcal{L}$, let $\mathbf{K}_{m,l} \in \mathbb{C}^{N\times N}$ be the $(m,[m-l]_M)$-th subblock of the channel matrix $\mathbf{H}$. Accordingly, the per-block DD domain input-output expression is [22, Ch. 4]

$$\mathbf{y}_m = \sum_{l\in\mathcal{L}} \mathbf{K}_{m,l}\mathbf{x}_{[m-l]_M} + \mathbf{w}_m \tag{14}$$

The subblock $\mathbf{K}_{m,l}$ is circulant [22]:

$$\mathbf{K}_{m,l} = \mathsf{circ}[\boldsymbol{\nu}_{m,l}(0),\cdots,\boldsymbol{\nu}_{m,l}(N-1)] \,, \tag{15}$$

with the discrete Doppler spread vector $\boldsymbol{\nu}_{m,l} \in \mathbb{C}^N$ given by

$$\begin{aligned} \boldsymbol{\nu}_{m,l}(k) \;\; &= \;\; \frac{1}{N}\sum_{\ell\in\mathcal{L}}\left(\sum_{\kappa\in\mathcal{K}_\ell} \nu_\ell(\kappa) z^{\kappa(m-l)} \vartheta_N(\kappa\eta_g - k)\right) \\ &\quad \times \operatorname{sinc}(l-\ell), \end{aligned} \tag{16}$$

where $z = e^{\jmath\frac{2\pi}{NM}}$ and $\eta_g = (1 + \frac{l_g}{M})$. The function

$$\vartheta_N(x) = \frac{\sin(\pi x)}{\sin(\pi x/N)} \mathrm{e}^{\jmath\frac{\pi x(N-1)}{N}} \tag{17}$$

encapsulates additional phase and magnitude variations induced by fractional Doppler shifts. In practical systems, fractional delays are often ignored because the sampling resolution $1/M\Delta_f$ typically suffices to approximate any delays by their nearest integer sample indices. Assuming integer delays $\ell \in \mathbb{Z}$, the sinc term in (16) becomes $\delta[l-\ell]$.

III. SPECTRAL PRECODER DESIGNS

We assume QAM symbols in each frame are zero-mean, proper, uncorrelated (both within and across frames), and have unit variance. From [23, Th. 1], the OTFS baseband signal is cyclostationary with period $T_u + T_g$ and its power spectral density (PSD) is

$$\mathrm{P_s}(f) = |\mathrm{H_I}(f)|^2 \boldsymbol{\phi}^{\mathsf{H}}(f)\mathbf{G}_{\mathrm{TF}}\mathbf{G}_{\mathrm{TF}}^{\mathsf{H}}\boldsymbol{\phi}(f), \tag{18}$$

where $\mathbf{G}_{\mathrm{TF}} = \mathbf{F}_M\mathbf{G}_{\mathrm{DD}}$ is the TF domain precoder, $\mathrm{H_I}(f)$ is the frequency response of the DAC interpolation filter, and $\boldsymbol{\phi}(f) \in \mathbb{C}^M$ contains the responses of active subcarriers [19]. Given a weighting function $\mathrm{W}(f) \geq 0$, the weighted transmit power is defined as

$$\mathrm{P_W} \triangleq \int_{-\infty}^{+\infty} \mathrm{W}(f)\mathrm{P_s}(f)\mathrm{d}f \;=\; \mathsf{tr}\Big(\mathbf{G}_{\mathrm{TF}}^{\mathsf{H}}\boldsymbol{\Phi}\mathbf{G}_{\mathrm{TF}}\Big), \tag{19}$$

with the Hermitian positive semi-definite matrix

$$\boldsymbol{\Phi} \triangleq \int_{-\infty}^{+\infty} \mathrm{W}(f)|\mathrm{H_I}(f)|^2\boldsymbol{\phi}(f)\boldsymbol{\phi}^{\mathsf{H}}(f)\mathrm{d}f. \tag{20}$$

An appropriate choice of $\mathrm{W}(f)$ allows for a flexible definition of OBR; *e.g.,* setting $\mathrm{W}(f) = 1$ for $f \in \mathcal{B}$ (the band of interest) and 0 elsewhere.

We consider two classical spectral precoder designs from OFDM, namely AIC and orthogonal precoding (OP), to minimize $\mathrm{P_W}$ in (19), each subject to different structural constraints on the TF-domain matrix $\mathbf{G}_{\mathrm{TF}}$ [19]. Following [7], [8], the AIC precoder is of the form $\mathbf{G}_{\mathrm{TF}} \triangleq \alpha\,\mathbf{E} + \mathbf{T}\,\boldsymbol{\Theta}$, where $\mathbf{E} \in \mathbb{C}^{M\times D}$ and $\mathbf{T} \in \mathbb{C}^{M\times R}$ are fixed selection matrices (columns of $\mathbf{I}_M$) for data and cancellation subcarriers, resp., and $\boldsymbol{\Theta}$ is optimized to minimize $\mathrm{P_W}$, subject to a transmit power constraint. Under OP [9], [10], the columns of $\mathbf{G}_{\mathrm{TF}}$ are constrained to be orthonormal, so $\mathrm{P_W}$ is minimized by picking the D least dominant eigenvectors of $\boldsymbol{\Phi}$.

IV. PROPOSED DECODER

Using the DD domain input-output relation (14), we extend the iterative DD-MRC detection framework from [17] to CP-OTFS accounting for spectral precoding. The proposed MRC receiver in the DD domain is formulated as follows. First, as per [17], the initial symbol estimates are obtained in the TF-domain by means of a single-tap MMSE equalizer. These initial estimates are then mapped to the DD-domain by the SFFT operation, yielding $\hat{\mathbf{x}}_0^{(0)}, \hat{\mathbf{x}}_1^{(0)}, \ldots, \hat{\mathbf{x}}_{M-1}^{(0)}$. With these, we compute the residual noise plus interference (RNPI) vectors due to noise and imperfect symbol estimation:

$$\Delta\mathbf{y}_m^{(0)} = \mathbf{y}_m - \sum_{l'\in\mathcal{L}} \mathbf{K}_{m,l'}\hat{\mathbf{x}}_{[m-l']_M}^{(0)}. \tag{21}$$

Thus, at iteration $i \geq 1$, the DD-domain symbol estimates and RNPI vectors $\{\hat{\mathbf{x}}_m^{(i-1)}, \Delta\mathbf{y}_m^{(i-1)}, m \in \mathcal{M}\}$ are available. Then, for $m = 0, 1, \ldots, M-1$:

1) Set the RNPI vectors to those from the previous iteration:

$$\Delta\mathbf{y}_m^{(i)} = \Delta\mathbf{y}_m^{(i-1)}, \quad m \in \mathcal{M}. \tag{22}$$

2) Extract the channel-impaired component of $\mathbf{x}_m$ at l-th delay tap, $l \in \mathcal{L}$, denoted as $\mathbf{b}_{m,l}^{(i)}$:

$$\begin{aligned}\mathbf{b}_{m,l}^{(i)} &= \mathbf{y}_{[m+l]_M} - \sum_{l'\in\mathcal{L}, l'\neq l} \mathbf{K}_{[m+l]_M,l'}\hat{\mathbf{x}}_{[m+l-l']_M}^{(i')} \\ &= \mathbf{K}_{[m+l]_M,l}\hat{\mathbf{x}}_m^{(i-1)} + \Delta\mathbf{y}_{[m+l]_M}^{(i-1)},\end{aligned} \tag{23}$$

where $i' = i$ if $[m+l-l']_M < m$, and $i' = i-1$ otherwise.

3) Compute the MRC output, which serves as a refined soft estimate at the i-th iteration

$$\begin{aligned}\mathbf{c}_m^{(i)} &= \boldsymbol{\Lambda}_m^{-1}\sum_{l\in\mathcal{L}} \mathbf{K}_{[m+l]_M,l}^{\mathsf{H}}\mathbf{b}_{m,l}^{(i)} \\ &= \hat{\mathbf{x}}_m^{(i-1)} + \boldsymbol{\Lambda}_m^{-1}\sum_{l\in\mathcal{L}} \mathbf{K}_{[m+l]_M,l}^{\mathsf{H}}\Delta\mathbf{y}_{[m+l]_M}^{(i)},\end{aligned} \tag{24}$$

where $\boldsymbol{\Lambda}_m = \sum_{l\in\mathcal{L}} \mathbf{K}_{[m+l]_M,l}^{\mathsf{H}}\mathbf{K}_{[m+l]_M,l}$ is the aggregate channel gain associated with the transmitted symbol $\mathbf{x}_m$.

4) To obtain *hard* estimates, the finite cardinality property of the QAM constellation is to be used, for which it becomes necessary to undo the effect of the spectral precoder. Thus, using the refined estimate (24), we first construct the matrix $\mathbf{Z}_{m,i} \in \mathbb{C}^{M\times N}$ as

$$\mathbf{Z}_{m,i} = \Big[\hat{\mathbf{x}}_0^{(i)} \cdots \hat{\mathbf{x}}_{m-1}^{(i)}\; \mathbf{c}_m^{(i)}\; \hat{\mathbf{x}}_{m+1}^{(i-1)} \cdots \hat{\mathbf{x}}_{M-1}^{(i-1)}\Big]^{\mathsf{T}}, \tag{25}$$

which is the current estimate of $\mathbf{X}_{\mathrm{DD}} = \mathbf{G}_{\mathrm{DD}}\mathbf{Q} = \mathbf{F}_M^{\mathsf{H}}\mathbf{G}_{\mathrm{TF}}\mathbf{Q}$. The corresponding estimate of $\mathbf{Q}$ is then[1]

$$\boldsymbol{\Gamma}_{m,i} = \mathbf{G}_{\mathrm{DD}}^{\dagger}\mathbf{Z}_{m,i} = \begin{cases} \mathbf{G}_{\mathrm{TF}}^{\mathsf{H}}\mathbf{F}_M\mathbf{Z}_{m,i}, & \text{(OP)} \\ \alpha^{-1}\mathbf{E}^{\mathsf{H}}\mathbf{F}_M\mathbf{Z}_{m,i}. & \text{(AIC)}\end{cases} \tag{26}$$

Letting $\boldsymbol{\zeta}_m = \mathbf{G}_{\mathrm{DD}}^{\mathsf{T}}\mathbf{e}_m$, and noting that the m-th row of $\mathbf{X}_{\mathrm{DD}}$ is given by $\mathbf{x}_m = \mathbf{X}_{\mathrm{DD}}^{\mathsf{T}}\mathbf{e}_m = \mathbf{Q}^{\mathsf{T}}\boldsymbol{\zeta}_m$, a hard estimate of $\mathbf{x}_m$ can be obtained as $\mathsf{DEC}\{\boldsymbol{\Gamma}_{m,i}^{\mathsf{T}}\}\,\boldsymbol{\zeta}_m$.

5) To improve both performance and convergence, a damping factor $\lambda \in [0,1]$ is introduced, so that the final estimate is a convex combination of soft and hard estimates:

$$\hat{\mathbf{x}}_m^{(i)} = (1-\lambda)\mathbf{c}_m^{(i)} + \lambda\mathsf{DEC}\Big\{\boldsymbol{\Gamma}_{m,i}^{\mathsf{T}}\Big\}\,\boldsymbol{\zeta}_m, \tag{27}$$

6) For all $l \in \mathcal{L}$, update $\Delta\mathbf{y}_{[m+l]_M}^{(i)}$ using the most recent estimate $\hat{\mathbf{x}}_m^{(i)}$:

$$\Delta\mathbf{y}_{[m+l]_M}^{(i)} \leftarrow \Delta\mathbf{y}_{[m+l]_M}^{(i)} - \mathbf{K}_{[m+l]_M,l}(\hat{\mathbf{x}}_m^{(i)} - \hat{\mathbf{x}}_m^{(i-1)}). \tag{28}$$

7) Increment m and repeat steps 1 to 6 for $m \in \mathcal{M}$.

8) Stop if the maximum number of iterations is reached or the relative change in RNPI vector norm falls below a specified threshold.

Ultimately, a final hard decision is applied to obtain $\hat{\mathbf{Q}} = \mathsf{DEC}\Big\{\mathbf{G}_{\mathrm{DD}}^{\dagger}\hat{\mathbf{X}}_{\mathrm{DD}}\Big\}$, where $\hat{\mathbf{X}}_{\mathrm{DD}} = [\hat{\mathbf{x}}_0^{(I)} \cdots \hat{\mathbf{x}}_{M-1}^{(I)}]^{\mathsf{T}}$, with I the index of the last iteration.

[1]For AIC, (26) is due to the fact that $\mathbf{E}^{\mathsf{H}}\mathbf{E} = \mathbf{I}_D$ and $\mathbf{E}^{\mathsf{H}}\mathbf{T} = \mathbf{0}$.

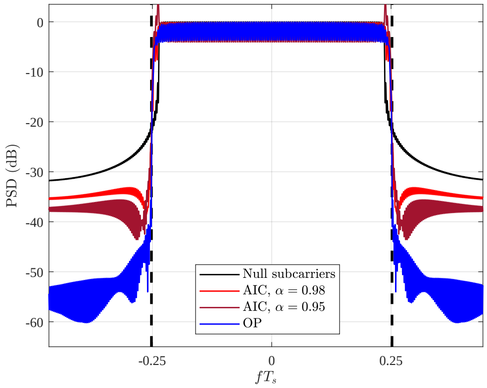

Fig. 2: PSDs for various precoder designs. $M = 128$, $N = 64$, $l_g = \lfloor \frac{M}{16} \rfloor$, precoder redundancy $R = 6$, using 4-QAM.

Computational Complexity

Relative to the original (without spectral precoding) DD-MRC detector, additional operations are required in steps 4 and 5 only, and only for $\lambda \neq 0$. In this regard, note that $\mathbf{Z}_{m,i}$ differs from $\mathbf{Z}_{m-1,i}$ only in its $(m-1)$-th and m-th rows:

$$\mathbf{Z}_{m,i} = \mathbf{Z}_{m-1,i} + (\mathbf{e}_m \boldsymbol{\delta}_{m,i}^{\mathsf{T}} - \mathbf{e}_{m-1} \boldsymbol{\varepsilon}_{m-1,i}^{\mathsf{T}}). \tag{29}$$

where $\boldsymbol{\varepsilon}_{m,i} \triangleq \mathbf{c}_m^{(i)} - \hat{\mathbf{x}}_m^{(i)}$ and $\boldsymbol{\delta}_{m,i} \triangleq \mathbf{c}_m^{(i)} - \hat{\mathbf{x}}_m^{(i-1)}$. Hence, upon defining $\mathbf{f}_m \triangleq \mathbf{G}_{\mathrm{DD}}^{\dagger} \mathbf{e}_m = \mathbf{G}_{\mathrm{TF}}^{\dagger} \mathbf{F}_M \mathbf{e}_m$ (so that $\mathbf{f}_m = \boldsymbol{\zeta}_m^*$ for OP, and $\mathbf{f}_m = \alpha^{-1} \mathbf{E}^{\mathsf{H}} \mathbf{F}_M \mathbf{e}_m$ for AIC) one has:

$$\boldsymbol{\Gamma}_{m,i} = \boldsymbol{\Gamma}_{m-1,i} + (\mathbf{f}_m \boldsymbol{\delta}_{m,i}^{\mathsf{T}} - \mathbf{f}_{m-1} \boldsymbol{\varepsilon}_{m-1,i}^{\mathsf{T}}), \tag{30}$$

requiring $\mathcal{O}(ND)$ complex products. Thus, per iteration complexity for $\lambda = 0$ is $\mathcal{O}(M(N^3 + N^2 L))$, matching that of the original scheme [17]; whereas for $\lambda > 0$, the corresponding figure is $\mathcal{O}(M(N^3 + N^2 L + ND))$. Note, the spectral precoder-aware DT-MRC detector from [19] has complexity $\mathcal{O}(NMD)$ for $\lambda > 0$, and the LMMSE equalizer for CP-OTFS has complexity $\mathcal{O}(N^3 M^3)$, reducible to $\mathcal{O}(NML^2)$ by exploiting channel sparsity [24]. Although the proposed DD-MRC detector is computationally heavier, it outperforms its forerunners in terms of error rate, as shown next.

V. Results and Discussion

We consider a CP-OTFS system with $\Delta_f = 15$ kHz and CP redundancy $T_{\mathrm{cp}}/T_{\mathrm{u}} = 1/16$, yielding $T_{\mathrm{cp}} \approx 4$ μs. The channel is modeled using EVA profile [25] with $L = 9$ propagation paths and a speed of 120 km/h. Each path γ experiences a single Doppler shift given by $\nu_\gamma = \nu_{\max} \cos(\theta_\gamma)$ where $\theta_\gamma \sim U[-\pi, \pi]$. The maximum Doppler shift $\nu_{\max}$ is chosen so that $NT_u \nu_{\max} = \kappa_{\max} = 4$; whereas the maximum delay spread is limited to 5 taps, *i.e.*, $l_{\max} = 4$, ensuring that $\tau_{\max} \leq T_{\mathrm{cp}}$ for $M \geq 64$. We assume that perfect channel state information is available at the receiver. Unless otherwise specified, the damping factor λ is set to 0.2.

A. Spectral performance

Consider a setting with frame length $N = 64$ and $M = 128$ active subcarriers. The oversampling factor is $F = 2$ ($K = 256$, $T_s = T/2$), and the DAC filter is assumed to be an ideal lowpass with cutoff frequency $\frac{1}{2T_s}$. The OBR region is $\mathcal{B} = \left\{ \frac{1}{4T_s} + \frac{\Delta f}{2} \leq |f| \leq \frac{1}{2T_s} \right\}$. A uniform weighting function is applied: $W(f) = 1$ for $f \in \mathcal{B}$, and zero elsewhere.

Fig. 2 depicts the PSDs obtained by different precoding schemes with $R = 6$. With OP, OBR is reduced by 25.6 dB relative to the unprecoded case, which employs $R/2$ null subcarriers per band edge, *i.e.*, equivalent to AIC with $\boldsymbol{\Theta} = \mathbf{0}$. With AIC, the OBR reduction is 3.6 dB for $\alpha = 0.98$ and 6.1 dB for $\alpha = 0.95$, as lower α values allocate more power to cancellation subcarriers. However, with smaller α spectral peaks within the passband increase, potentially violating spectral emission constraints. Thus, optimizing α requires balancing OBR suppression and spectral overshoot.

Whereas OP is much more effective than AIC in terms of OBR reduction, in OFDM the latter is completely transparent at the receiver, which simply discards cancellation subcarriers. However, this feature is lost in OTFS, where receiver complexity is similar for OP and AIC. Thus, there seems to be little incentive for the adoption of AIC in OTFS systems.

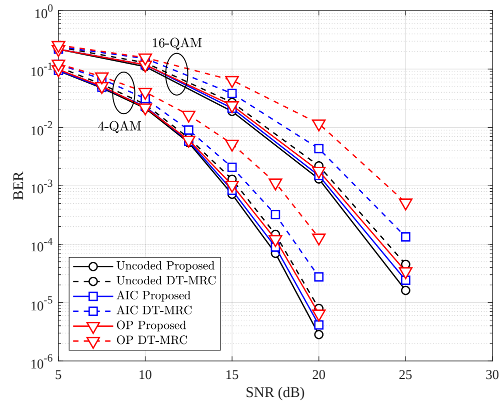

(a) $N = 32$, $M = 64$

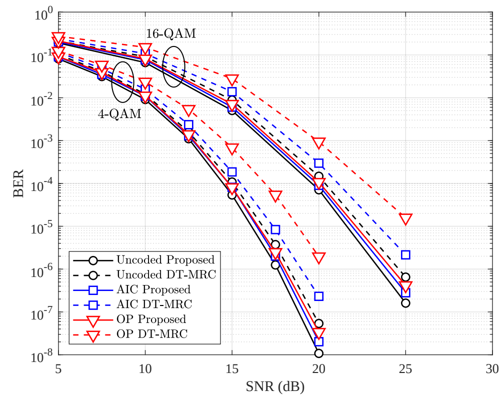

(b) $N = 64$, $M = 128$

Fig. 3: BER for different precoders and frame sizes: proposed DD-MRC vs DT-MRC detectors.

B. BER Performance

Fig. 3 shows BER curves for the proposed detector with 4-QAM and 16-QAM and different spectral precoders with

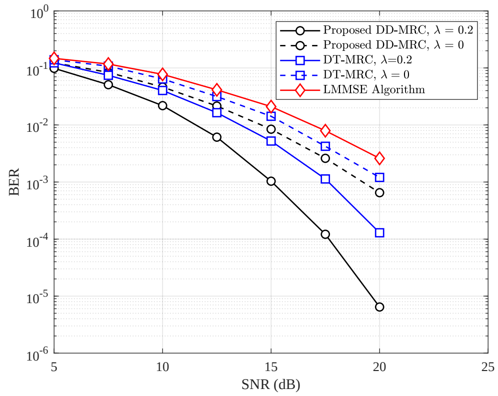

Fig. 4: BER performance: proposed DD-MRC vs. DT-MRC vs. LMMSE detectors. $N = 32$, $M = 64$, 4-QAM, OP ($R = 6$).

$R = 6$. The performance is compared with the state-of-the-art spectral precoder-aware DT-MRC detector from [19]. Two different frame sizes are considered: $(N, M) = (32, 64)$ in Fig. 3(a), and $(N, M) = (64, 128)$ in Fig. 3(b). In all cases, the proposed DD-MRC detector outperforms its DT-MRC counterpart. Moreover, the differences in BER over the different spectral precoding schemes are minor, in contrast with the DD-MRC detector, which exhibits a definite tradeoff between OBR reduction and BER performance.

Fig. 4 shows the BER obtained with the proposed DD-MRC detector, the DT-MRC detector from [19], and the scheme from [15], adapted for CP-OTFS. The last method applies LMMSE equalization in the time domain, followed by a transformation to the DD domain, and finally spectral decoding using the pseudoinverse $\mathbf{G}_{\mathrm{DD}}^{\dagger}$. The advantage of the proposed scheme is clear; even in the case $\lambda = 0$ (*i.e.,* the iteration is based on soft estimates only), DD-MRC still outperforms the scheme from [15].

VI. Conclusions

Spectral precoding is an effective technique to shape the spectrum of multicarrier signals, and can be applied to OTFS. However, the impact of spectral precoding in the detection process at the receiver must be carefully considered. Whereas previous approaches suffer a significant loss in terms of BER once spectral precoding is introduced, this drawback is overcome with the proposed delay-Doppler domain detector. Moreover, BER performance is not affected by the type of spectral precoder. These benefits come at the price of increased computational complexity, and therefore devising reduced-complexity approaches with good BER and sidelobe reduction is a problem of definite interest.

Acknowledgment

Work funded by MCIN/AEI/10.13039/501100011033/ FEDER "A way of making Europe" under project MAYTE (PID2022-136512OB-C22).

References

[1] Z. Wei, W. Yuan, S. Li, J. Yuan, G. Bharatula, R. Hadani, and L. Hanzo, "Orthogonal time-frequency space modulation: A promising next-generation waveform," *IEEE Trans. Wireless Commun.*, vol. 28, no. 4, pp. 136–144, 2021.

[2] R. Hadani, S. Rakib, M. Tsatsanis, A. Monk, A. J. Goldsmith, A. F. Molisch, and R. Calderbank, "Orthogonal time frequency space modulation," in *IEEE Wireless Commun. Netw. Conf. (WCNC)*, 2017.

[3] P. Raviteja, K. T. Phan, Y. Hong, and E. Viterbo, "Interference cancellation and iterative detection for OTFS modulation," *IEEE Trans. Wireless Commun.*, vol. 17, no. 10, pp. 6501–6515, 2018.

[4] M. Faulkner, "The effect of filtering on the performance of OFDM systems," *IEEE Trans. Veh. Technol.*, vol. 49, pp. 1877–1884, 2000.

[5] R. Zayani, Y. Medjahdi, H. Shaiek, and D. Roviras, "WOLA-OFDM: A potential candidate for asynchronous 5G," in *IEEE Globecom Workshops (GC Wkshps)*, 2016.

[6] K. Hussain and R. López-Valcarce, "Optimal window design for W-OFDM," in *IEEE Int. Conf. Acoust., Speech Signal Process. (ICASSP)*, 2020, pp. 5275–5289.

[7] S. Brandes, I. Cosovic, and M. Schnell, "Reduction of out-of-band radiation in OFDM systems by insertion of cancellation carriers," *IEEE Commun. Lett.*, vol. 10, no. 6, pp. 420–422, 2006.

[8] J. Schmidt, S. Costas-Sanz, and R. López-Valcarce, "Choose your subcarriers wisely: Active interference cancellation for cognitive OFDM," *IEEE J. Emerg. Sel. Topics Circuits Syst.*, vol. 3, pp. 615–625, 2013.

[9] M. Ma, X. Huang, B. Jiao, and Y. J. Guo, "Optimal orthogonal precoding for power leakage suppression in DFT-based systems," *IEEE Commun. Lett.*, vol. 59, no. 3, pp. 844–853, 2011.

[10] R. Kumar, K. Hussain, and R. López-Valcarce, "Mask-compliant orthogonal precoding for spectrally efficient OFDM," *IEEE Trans. Commun.*, vol. 69, no. 3, pp. 1990–2001, 2021.

[11] C.-D. Chung, "Spectrally precoded OFDM," *IEEE Trans. Commun.*, vol. 54, no. 12, pp. 2173–2185, 2006.

[12] K. Hussain, R. López-Valcarce, F. Rey, J. Sala-Alvarez, and J. Villares, "Sidelobe suppression for multicarrier signals via structured spectral precoding," *IEEE Trans. Commun.*, vol. 72, no. 6, pp. 3155–3168, 2024.

[13] A. Farhang, A. RezazadehReyhani, L. E. Doyle, and B. Farhang-Boroujeny, "Low complexity modem structure for OFDM-based orthogonal time frequency space modulation," *IEEE Wireless Commun. Lett.*, vol. 7, no. 3, pp. 344–347, 2018.

[14] M. N. Hossain, Y. Sugiura, T. Shimamura, and H.-G. Ryu, "Waveform design of low complexity WR-OTFS system for OOB power reduction," in *IEEE Wireless Commun. Netw. Conf. Workshops (WCNCW)*, 2020.

[15] W.-C. Chen, C.-H. Lu, and C.-D. Chung, "Spectrally precoded OTFS modulation," in *IEEE 96th Veh. Technol. Conf. (VTC-Fall)*, 2022.

[16] Y. Zhu, Z. Wang, and Z. Liu, "Optimal column inversion precoding for PAPR reduction in SP-OTFS system," in *IEEE/CIC Int. Conf. Commun. China (ICCC Workshops)*, 2024, pp. 553–557.

[17] T. Thaj and E. Viterbo, "Low complexity iterative rake decision feedback equalizer for zero-padded OTFS systems," *IEEE Trans. Veh. Technol.*, vol. 69, no. 12, pp. 15 606–15 622, 2020.

[18] T. Thaj, E. Viterbo, and Y. Hong, "General I/O relations and low-complexity universal MRC detection for all OTFS variants," *IEEE Access*, vol. 10, pp. 96 026–96 037, 2022.

[19] V. Vahidpour and R. López-Valcarce, "Spectral precoding integration in OTFS modulation," in *IEEE Wireless Commun. Netw. Conf. (WCNC)*, 2025, pp. 1–6.

[20] B. Farhang-Boroujeny, *Signal Processing Techniques for Software Radios*. Lulu Publishing House, 2010.

[21] P. Raviteja, Y. Hong, E. Viterbo, and E. Biglieri, "Practical pulse-shaping waveforms for reduced-cyclic-prefix OTFS," *IEEE Trans. Veh. Technol.*, vol. 68, no. 1, pp. 957–961, 2019.

[22] Y. Hong, T. Thaj, and E. Viterbo, *Delay-Doppler Communications: Principles and Applications*. Academic Press, 2022.

[23] R. López-Valcarce, "General form of the power spectral density of multicarrier signals," *IEEE Commun. Lett.*, vol. 26, no. 8, pp. 1755–1759, 2022.

[24] S. Tiwari, S. S. Das, and V. Rangamgari, "Low complexity LMMSE receiver for OTFS," *IEEE Commun. Lett.*, vol. 23, no. 12, pp. 2205–2209, 2019.

[25] "LTE evolved universal terrestrial radio access (E-UTRA); base station (BS) radio transmission and reception," *3GPP TS 36.104 version 8.6.0 Release 8*, Jul. 2009.